

Shapiro steps observed in a two-dimensional Yukawa solid modulated by a one-dimensional vibrational periodic substrate

Zhaoye Wang¹, Nichen Yu¹, C. Reichhardt², C. J. O. Reichhardt², Ao Xu¹, Xin Chen¹, and Yan Feng^{1,*}

¹ *Institute of Plasma Physics and Technology, Jiangsu Key Laboratory of Frontier Material Physics and Devices, School of Physical Science and Technology, Soochow University, Suzhou 215006, China*

² *Theoretical Division, Los Alamos National Laboratory, Los Alamos, New Mexico 87545, USA*

(Dated: January 8, 2025)

Depinning dynamics of a two-dimensional (2D) solid dusty plasma modulated by a one-dimensional (1D) vibrational periodic substrate are investigated using Langevin dynamical simulations. As the uniform driving force increases gradually, from the overall drift velocity varying with the driving force, four significant Shapiro steps are discovered. The data analysis indicate that, when the ratio of the frequency from the drift motion over potential wells to the external frequency from the modulation substrate is close to integers, dynamic mode locking occurs, corresponding to the discovered Shapiro steps. Around both termini of the first and fourth Shapiro steps, the transitions are found to be always continuous, however, the transition between the second and third Shapiro steps is discontinuous, probably due to the different arrangements of particles.

I. INTRODUCTION

Collective dynamics of interacting particles under substrate modulation have been extensively studied in various physical systems, such as colloids [1], vortex lattices in type-II superconductors [2], pattern-forming systems [3], Wigner crystals [4], and dusty plasmas [5]. While driven by a uniform force with different magnitudes, these substrate-modulated systems exhibit interesting depinning dynamics [5, 6], e.g., three dynamical states of the pinned, disordered plastic flow, and moving ordered can be observed. Besides these three dynamical states, depinning dynamics also include more interesting phenomena, including kinks and antikinks [7], superlubricity or the Aubry transition [8], directional locking [9], and Shapiro steps [10].

Shapiro steps are one of prominent characteristics commonly observed in nonlinear depinning dynamical systems with competing timescales [11]. When particles move over a periodic substrate by a uniform driving force, the drift velocity of the particles increases with the driving force, so does the frequency of the drift motion over potential wells. When an additional alternating current (AC) frequency is introduced into the driving force or the substrate, the coupling between these two frequencies leads to new dynamics phenomena [10]. Especially, when the introduced AC frequency is synchronized with the frequency of the drift motion over potential wells, particles' drift velocity remains constant within certain driving force intervals due to resonance [12], forming a series of steps known as the Devil's staircases [13] or the Shapiro steps [10]. The Shapiro steps have been observed in various systems, such as Josephson junctions [14, 15], vortices in type-II superconductors [16–18], charge-density waves [19, 20], colloids [10], skyrmions [21], and Frenkel-Kontorova models [22].

As a prominent experimental model system, dusty plasma, also termed as complex plasma, is composed of ions, electrons, neutral gas atoms, and micron-sized dust particles [23–43]. Under the typical laboratory conditions, these micron-sized dust particles are highly charged to $\approx 10^4$ elementary charges negatively in plasma, interacting with each other through the Yukawa repulsion [44] of $\phi_{ij} = Q^2 \exp(-r_{ij}/\lambda_D)/4\pi\epsilon_0 r_{ij}$, where Q is the charge on each particle, r_{ij} is the distance between two particles, and λ_D is the Debye screening length. These charged dust particles can be suspended and confined by the electric field in the plasma sheath, self-organizing into a single-layer, i.e., a two-dimensional (2D) dusty plasma [45, 46]. Due to their high charges, these dust particles are strongly coupled to each other, exhibiting the typical solid [39, 47, 48] and liquid like [47–49] properties. Using various manipulations, such as powerful laser beams [39, 50] or stripe electrodes [51], the dynamics of these dust particles can be easily modulated in experiments. While moving in plasma, these dust particles also experience a weak frictional gas damping [52]. In 2D dusty plasma experiments, the motion of dust particles can be recorded by video imaging [39, 50] and then accurately analyzed using particle tracking velocimetry [53–56]. Thus, dusty plasma can be used to study various fundamental physical procedures of solids and liquids at the individual particle level, including shocks [57], diffusion [58], phase transitions [30, 59–61], and internal friction [62].

Recently, the depinning dynamics of 2D dusty plasmas modulated by periodic substrates have been intensively investigated using computer simulations [5, 63–66]. From Ref. [5], when a gradually increasing uniform driving force is applied to substrate-modulated 2D dusty plasmas, the pinned state, the disordered plastic flow, and the moving ordered state are all observed. Besides these three dynamical states, other dynamical behaviors are also found, including the directional locking [63], the superlubric-pinned transition [65], and the bidirectional flow [67]. However, from our literature search, the

* The author to whom correspondence may be addressed: fengyan@suda.edu.cn

Shapiro steps have not been found in the previous investigations of dusty plasmas or Yukawa systems, as we study here.

The rest of this paper is organized as follows. In Sec. II, we briefly describe our computer simulation method of 2D solid dusty plasma modulated by a 1D vibrational periodic substrate and also driven by a uniform force. In Sec. III, we present our discovered Shapiro steps in the substrate-modulated 2D Yukawa solid. We also investigate the continuous/discontinuous transitions around both termini of each Shapiro step, using various structural and dynamical diagnostics. Finally, we provide a summary of these findings in Sec. IV.

II. SIMULATION METHODS

To characterize our studied 2D dusty plasmas, we follow [68] to use two dimensionless parameters, which are the coupling parameter Γ and the screening parameter κ [35, 68–70]. They are defined as $\Gamma = Q^2/4\pi\epsilon_0ak_B T$ [68] and $\kappa = a/\lambda_D$ [68], respectively. Here, T is the kinetic temperature of particles, $a = (n\pi)^{-1/2}$ is the Wigner-Seitz radius for the areal number density n . Clearly, Γ can be regarded as the inverse of the kinetic temperature. Note that, besides a , the lattice constant b is also used as the length unit, which is $\approx 1.90a$ for our studied 2D triangular lattice [68].

To investigate the Shapiro step in substrate-modulated 2D dusty plasmas, we perform Langevin dynamical simulations [5]. In our simulated 2D dusty plasmas with N_p particles, the equation of motion for each particle i is

$$m\ddot{\mathbf{r}}_i = - \sum \nabla\phi_{ij} - \nu m\dot{\mathbf{r}}_i + \zeta_i(t) + \mathbf{F}_s + \mathbf{F}_d. \quad (1)$$

Here, the first term on the right-hand-side (RHS) is the binary Yukawa repulsion [44] between two particles. The second term $-\nu m\dot{\mathbf{r}}_i$ on the RHS represent the frictional gas drag, which is proportional to the velocity of this particle [71]. The third term $\zeta_i(t)$ on the RHS is the Langevin random kicks coming from the fluctuation-dissipation theorem of $\langle \zeta_i(0)\zeta_i(t) \rangle = 2m\nu k_B T \delta(t)$ [60, 72]. The latter two terms of \mathbf{F}_s and \mathbf{F}_d represent the forces from the modulation substrate and the external driving force, respectively, both in units of $F_0 = Q^2/4\pi\epsilon_0a^2$, as explained in detail next.

In our current investigation, following [11], we specify a 1D vibrational periodic substrate as

$$U(x) = \frac{U_0}{(2\pi)^2} \left\{ 1 - \cos \left[\frac{2\pi}{w} (x - A \cos(2\pi f_s t)) \right] \right\}. \quad (2)$$

Here, U_0 and w are the strength and width of the applied potential well, in units of $Q^2/4\pi\epsilon_0a$ and b , respectively. Different from the previously applied substrates [5, 63–66] in dusty plasma investigations, here we apply a lateral periodic excitation $A \cos(2\pi f_s t)$ to the substrate potential [11], where A and f_s are the amplitude and frequency of the vibrational excitation. As a result, the substrate

force \mathbf{F}_s is derived analytically using $-\nabla U(x)$ and Eq. (2) as

$$\mathbf{F}_s = - \frac{U_0}{2\pi w} \sin \left[\frac{2\pi}{w} (x - A \cos(2\pi f_s t)) \right] \hat{\mathbf{x}}. \quad (3)$$

In our current investigation, we choose the constant values of $U_0 = 1.0Q^2/4\pi\epsilon_0a$, $w = b$, $A = 1.0a$, and $f_s = 0.2\omega_{pd}$ in the substrate expression of Eq. (2), where the nominal dusty plasma $\omega_{pd} = (Q^2/2\pi\epsilon_0ma^3)^{1/2}$ [68]. The driving force $\mathbf{F}_d = F_d\hat{\mathbf{x}}$ along the x direction is always specified to be uniform for all simulated particles as in [5, 63–66], whose magnitude varies from 0 to $0.1F_0$ with the interval of $10^{-3}F_0$.

Other simulation details are listed as follows. We specify the conditions of 2D dusty plasmas as $\Gamma = 1000$, $\kappa = 2$, corresponding to the typical solid state [73]. Our simulation box is $60.9a \times 52.8a$ with the periodic boundary conditions, containing $N_p = 1024$ particles. We guarantee that the periodic boundary conditions are well satisfied for our applied substrate, since the width of our simulation box just corresponds to 32 full potential wells. We specify the frictional gas damping $\nu = 0.027\omega_{pd}$, comparable to the typical value in 2D dusty plasma experiments [45]. We integrate Eq. (1) with a time step of $0.001\omega_{pd}^{-1}$, small enough for our studied conditions. For each simulation run, after the simulation system reaches its steady state, we record the particles' positions and velocities in the time duration of $\omega_{pd}t = 1.4 \times 10^5$, long enough to obtain the structure and dynamics information. Note, we also perform a few test runs with 4096 particles to confirm that our reported results here are independent of the system size.

III. RESULTS AND DISCUSSION

A. Shapiro steps

To investigate the Shapiro step problem in a substrate-modulated 2D Yukawa solid driven by uniform external forces, we first calculate the overall drift velocity along the x direction using $V_x = N_p^{-1} \langle \sum_{i=1}^{N_p} \mathbf{v}_i \cdot \hat{\mathbf{x}} \rangle$. Here, $\langle \rangle$ means the ensemble average, which is achieved using the mean of 2×10^4 frames for each reported data point. Note, we confirm that the overall drift velocity along the y direction V_y is negligible since the applied uniform external force F_d is always in the x direction.

As the major result of this paper, from our calculated drift velocity V_x , we discover four significant Shapiro steps while gradually increasing the uniform driving force on the substrate-modulated 2D Yukawa solid, as presented in Fig. 1. From Fig. 1, as F_d increases gradually from zero, our V_x results exhibit five distinctive steps, corresponding to $V_x/a\omega_{pd} = 0, 0.38, 0.76, 1.14,$ and 1.52 , labeled as $S_0, S_1, S_2, S_3,$ and S_4 , respectively. The first step S_0 represents the typical pinned state [5] from

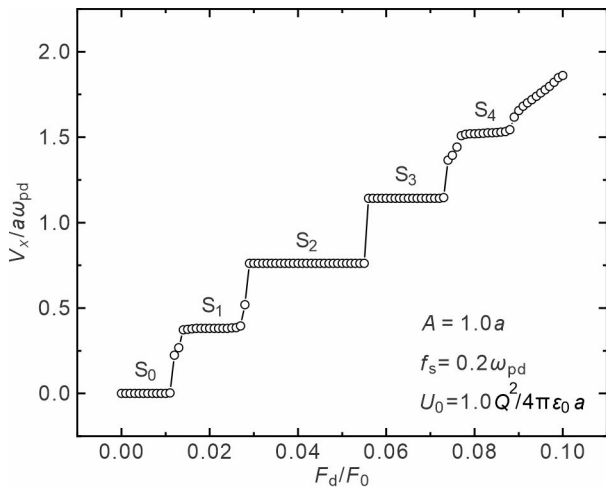


FIG. 1. Calculated collective drift velocity V_x of a 2D Yukawa solid modulated by a 1D vibrational substrate as a function of a uniform driving force F_d . As F_d increases from zero, the V_x results exhibit five distinctive steps, corresponding to $V_x/a\omega_{pd} = 0, 0.38, 0.76, 1.14,$ and 1.52 , labeled as $S_0, S_1, S_2, S_3,$ and S_4 , respectively. The first step S_0 corresponds to $V_x/a\omega_{pd} = 0$, i.e., all particles are confined inside the substrate, indicating the pinned state. While other four steps corresponding to the non-zero V_x values indicate the typical Shapiro steps, caused by the dynamic mode locking [12, 74]. Note, the conditions of the applied 1D vibrational substrate of Eq. (2) are $A = 1.0a$, $f_s = 0.2\omega_{pd}$, and $U_0 = 1.0 Q^2/4\pi\epsilon_0 a$.

$V_x = 0$, clearly indicating that all particles are pinned inside potential wells [5]. For a very large driving force of $F_d/F_0 \geq 0.09$, we find that V_x increases almost linearly with F_d with a fixed slope of $1/mv$, just corresponding to the typical moving ordered state [64], i.e., all particles move as a rigid body over the substrate with a constant speed [5]. Between these Shapiro steps, we also find some data points corresponding to the plastic flow state [5], as we will study later.

For the four Shapiro steps of $S_1, S_2, S_3,$ and S_4 in Fig. 1, although the applied driving force F_d increases substantially, i.e., $\geq 0.01F_0$, the overall drift velocity V_x remain constant, matching the definition of Shapiro steps [10]. From Fig. 1, the most prominent step is S_2 , with the varying range of $0.026F_0$ for F_d , much wider than those for other three. After S_2, S_3 is still more significant than S_1 and S_4 . Note, we also find that, at the two termini of S_2 and S_3 , the overall drift velocity V_x seems to change abruptly, however, at the two termini of S_1 or S_4 , V_x varies much more gradually.

Different from the previous studies [5, 63–65], the Shapiro steps discovered in the current investigation are mainly due to the specified lateral periodic excitation $A \cos(2\pi f_s t)$ of Eq. (3) on the substrate. In Refs. [5, 63–65] with the static modulation substrate, when uniform driving forces F_d are applied to 2D dusty plasmas or Yukawa systems, the three dynamical states of the pinned, disordered plastic flow, and moving ordered are

observed. While in our current investigation, the only difference is that the modulation substrate is vibrational from Eq. (2). As a result, when the driving force F_d increases gradually, besides the previously observed three states [5, 63–65], we also find one more dynamic state of the Shapiro steps.

In fact, Shapiro steps has also been observed in other systems, including Josephson junctions [14, 15], colloids [10, 74, 75], the Frenkel-Kontorova model [11, 12, 22, 76, 77], skyrmions [21, 78, 79], and vortex lattices [80]. Among these studies, some modulation substrates are vibrational [11, 74, 75], very similar to our 1D vibrational periodic substrate. While in other systems, although the modulation substrate is static, the driving force acting on particles is not uniform any more, which has an typical AC form of $A \cos(2\pi f_s t)$ [10, 12, 14, 15, 21, 22, 76–80]. From our understanding, to generate Shapiro steps, particles must experience an external AC excitation, either from the modulation substrate, or from the driving force, as we will discuss in detail later.

B. Dynamic mode locking

To investigate the underlying mechanism of our discovered Shapiro steps, we replot the calculated V_x results in different units of wf_s in Fig. 2(a). Surprisingly, the discovered four Shapiro steps always occur when V_x/wf_s just equals integers, i.e., $V_x = wf_s, 2wf_s, 3wf_s, 4wf_s$ for the 1st, 2nd, 3rd, 4th Shapiro steps, respectively. Note, within each Shapiro step, we always choose different conditions as two marked points $S_{n_s,A}$ and $S_{n_s,B}$ for the latter analysis. In Fig. 2(b), we present the calculated averaged displacement $\overline{\Delta x}$ within two periods under the conditions of our marked points in Fig. 2(a). From Fig. 2(b), our $\overline{\Delta x}$ results indicate that the displacement of all particles for the n_s th Shapiro step in one period is just $n_s w$, and the motion within each Shapiro step is exactly the same.

To intuitively describe the motion of particles under the conditions of the Shapiro steps, in Fig. 2(c), we plot the sketch of the microscopic mechanism from our understanding of Fig. 2(b). For the n_s th Shapiro step, particles laterally move forward n_s potential wells in the first period, then continue moving forward n_s potential wells in the second period, and so on. In fact, this microscopic mechanism is believed to be originated from the dynamic mode locking [75], as discussed next.

From Ref. [81], mode locking, also termed phase locking, refers to the resonance coupling between the free-running oscillator and an external driving force. In fact, dynamic mode locking is also named as synchronization [10, 81–83]. In our current investigation, as the uniform driving force increases, the frequency from the drift motion over potential wells increases simultaneously, while the external frequency f_s of the vibrational substrate is specified to be $0.2\omega_{pd}$. When the ratio of these two frequencies is close to a integer, the results in Fig. 2 clearly indicate the occurrence of dynamic mode locking

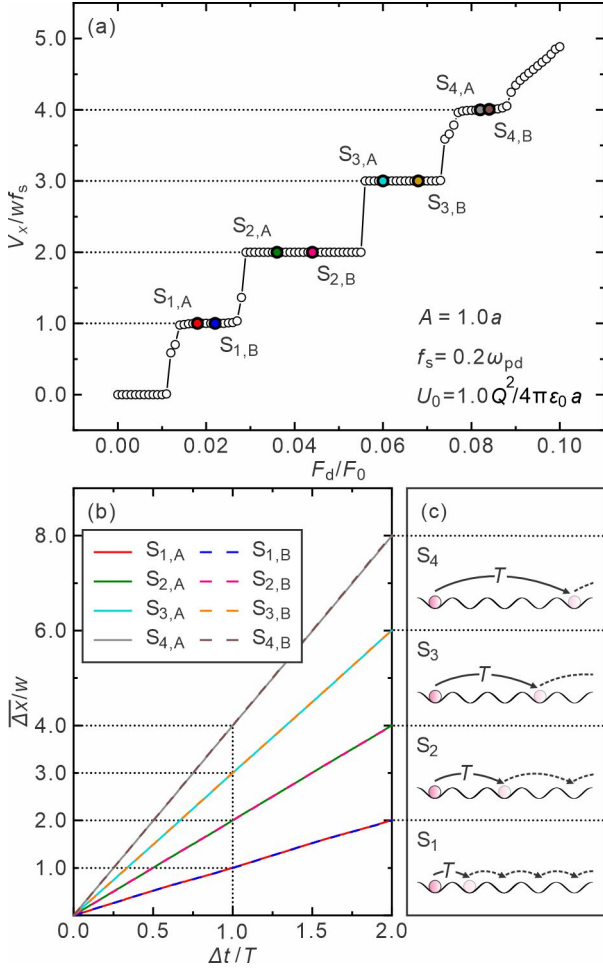


FIG. 2. The V_x values from Fig. 1 in units of wf_s (a), the corresponding particles' average displacements $\overline{\Delta x}$ (b), and sketches of the microscopic mechanism (c) for different Shapiro steps. Clearly, in units of wf_s , the Shapiro steps always occur when the V_x values are integers, i.e., $V_x / (wf_s) = 1, 2, 3,$ and 4 . As a result, the same results of $\overline{\Delta x}$ for $S_{n_s,A}$ and $S_{n_s,B}$ of each Shapiro step suggest that the average particle displacements are always $n_s w$ in one period, as shown in panel (b). Thus, the microscopic mechanism of each observed Shapiro step S_{n_s} just corresponds to the moving forward n_s potential wells in one period for all particles, as illustrated in panel (c).

under the conditions of the four Shapiro steps. Note, due to the synchronized motion of all particles under the Shapiro step conditions, the nominal dusty plasma frequency ω_{pd} does not play an important role any more.

To verify the dynamic mode locking of our observed Shapiro steps, we calculate the kinetic temperature $k_B T_y$ from the particle motion in the y direction, as presented in Fig. 3. Here, since our applied modulation substrate is in the x direction and also vibrational in the x direction, the kinetic temperature can be characterized using $k_B T_y = m \langle \sum_{i=0}^{N_p} (\mathbf{v}_{i,y} - \overline{\mathbf{v}}_y)^2 \rangle / 2$, in units of $Q^2 / 4\pi\epsilon_0 a$. From Fig. 3, clearly, there are four distinctive peaks in

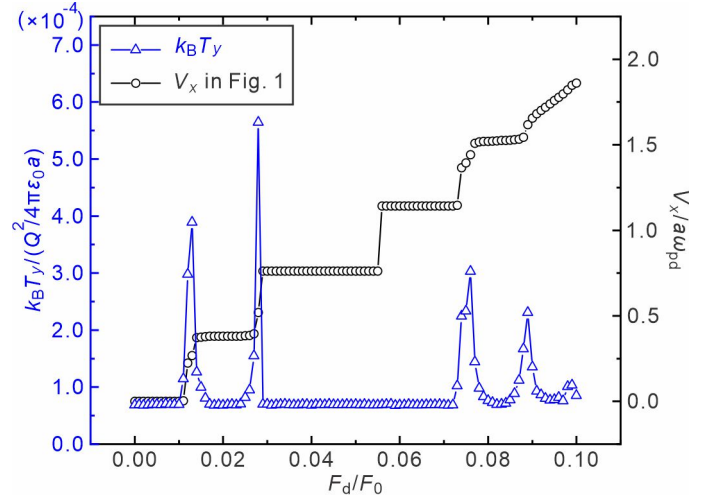


FIG. 3. Calculated kinetic temperature $k_B T_y$ and the drift velocity V_x in Fig. 1 as functions of the driving force F_d . The $k_B T_y$ results exhibit four distinctive peaks around both termini of the first and fourth Shapiro steps, i.e., S_1 and S_4 . However, under other conditions, the dimensionless kinetic temperature $k_B T_y / (Q^2 / 4\pi\epsilon_0 a)$ is only around 0.7×10^{-4} , much lower than values around those four peaks. These four peaks of $k_B T_y$ probably suggest the continuous transitions related to the first and fourth Shapiro steps.

the profile of $k_B T_y$, which are just located around both termini of S_1 and S_4 . Comparing the kinetic temperature results in Fig. 3 to the drift velocity V_x in Fig. 1, we find that these four peaks of $k_B T_y$ just correspond to the disordered plastic flow state at the two termini of S_1 and S_4 , respectively. Except for these four peaks, the dimensionless kinetic temperature $k_B T_y / (Q^2 / 4\pi\epsilon_0 a)$ for other conditions, including the four Shapiro steps, the pinned and moving ordered states, is always pretty low, only around 0.7×10^{-4} .

In Fig. 3, the relatively low level of the $k_B T_y$ results for the four Shapiro steps and the moving ordered states clearly reflect the velocity fluctuation among particles in the y direction is really tiny, i.e., the motion of all particles are synchronized. In our studied system, since the particle motion is modulated periodically in the x direction by the applied modulation substrate, we cannot use $k_B T_x = m \langle \sum_{i=0}^{N_p} (\mathbf{v}_{i,x} - \overline{\mathbf{v}}_x)^2 \rangle / 2$ to determine $k_B T_x$ directly. However, there is no modulation in the y direction, so that $k_B T_y$ is able to characterize the kinetic temperature of our studied system. From our understanding, under the conditions of each Shapiro step in Fig. 3, all particles move along the x direction in a synchronous and periodic fashion [75], leading to substantially reduced velocity fluctuations, or $k_B T_y$ equivalently. For the initial pinning and final moving ordered states, $k_B T_y$ results are almost at the same low level as those for Shapiro steps, since particles either only vibrate around their equilibrium locations or drift completely as a rigid object also in a synchronized manner, as described in

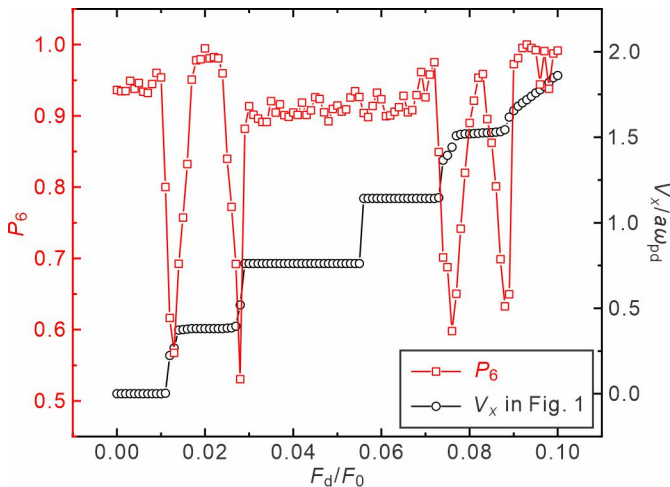


FIG. 4. Calculated results of the fraction of sixfold coordinated particles P_6 and the drift velocity V_x in Fig. 1 as functions of driving force F_d . The P_6 results exhibit four significant valleys around both termini of the S_1 and S_4 , corresponding to the disordered structure there. From our understanding, these four valleys suggest the continuous transitions related to the first and fourth Shapiro steps.

detail in Refs. [5, 64].

From our understanding, the four peaks of the $k_B T_y$ results in Fig. 3 are probably due to the continuous transition around the two termini of S_1 and S_4 . From Fig. 3, under the conditions of the disordered plastic flow state between Shapiro steps, the magnitude of $k_B T_y$ increases substantially to high values, even nearly 10 times of the value for the Shapiro steps. In fact, under the conditions of the four peaks of $k_B T_y$, the results of the drift velocity V_x also exhibit the gradual increase with F_d , corresponding to the continuous transition there, similar to the results in Ref. [64]. The only exception is the transition between S_2 and S_3 , where $k_B T_y$ remains at a low level while V_x abruptly changes from S_2 to S_3 , probably corresponding to a discontinuous transition [64], as discussed later.

C. Continuous and discontinuous transitions

To investigate the global structure of our studied system, we calculate the fraction of sixfold coordinated particles P_6 . From Ref. [1], P_6 is defined as $P_6 = N_p^{-1} \left\langle \sum_{i=1}^N \delta(6 - z_i) \right\rangle$, where z_i represents the coordination number of particle i determined through the Voronoi construction. When a 2D system varies from a perfect triangular lattice to a highly disordered liquid/gas, its P_6 value would decay from 1 to a low value close 0. We plot our calculated P_6 and V_x results as functions of F_d in Fig. 4 for the next analysis.

From Fig. 4, there are four distinctive valleys in the calculated P_6 profile, which are just located around both

termini of S_1 and S_4 . In fact, from the drift velocity V_x profile, these lower values of P_6 just correspond to the disordering plastic flow state. However, under the conditions of the four Shapiro steps, the pinned and moving ordered states, the P_6 value is pretty high, mostly higher than 0.9.

The relatively high values of P_6 in Fig. 4 indicate that the structure of our studied 2D Yukawa system is highly ordered. From Fig. 4, under the conditions of each Shapiro step, the relatively high values of P_6 clearly indicate the highly ordered structures there. For the conditions of Shapiro steps, the dynamic mode locking of the collective behaviors of particles means the synchronization motion of all particles. From our understanding, this synchronization reasonably leads to the highly ordered arrangement of particles, as indicated by the high values of P_6 in Fig. 4.

Under other conditions apart from the Shapiro steps, our studied substrate-modulated Yukawa system exhibits the similar depinning dynamics as in [5]. When $F_d/F_0 \leq 0.011$, the P_6 results are relatively high, while V_x remains nearly zero, corresponding to the pinned state, in which particles are aligned into 1D chains around the bottom of potential wells [5]. When $F_d/F_0 \geq 0.09$, the P_6 values are also pretty high, ≈ 0.95 , corresponding to the moving ordered state, in which all particles move in an orderly manner just like a rigid object [5]. Interestingly, the four valleys of the P_6 curves in Fig. 4 just correspond to the four transitions from S_0 to S_1 , S_1 to S_2 , S_3 to S_4 , and S_4 to the moving ordered state, which all belong to the plastic flow states [5]. Importantly, for the transition from S_2 to S_3 , P_6 always keeps at high values of ≈ 0.9 . In fact, in our simulations, although we use a much smaller increasing step of 10^{-5} for F_d/F_0 , a drop of P_6 between S_2 to S_3 has never been found, probably indicating the discontinuous transition there. However, other transitions around these Shapiro steps are always continuous instead from the significant drops of P_6 in Fig. 4.

To perform more detailed structure analysis of our studied system around the continuous/discontinuous transitions, we prepare histograms of the bond length $P_{\text{bond}}(r)$ using the Delaunay triangulation [84], as presented in Fig. 5. In Fig. 5(a), we mark night points for the conditions of the latter analysis in Figs. 5(b-j). Clearly, under the conditions on the Shapiro steps as in Figs. 5(b, f, g, h, i, j), the $P_{\text{bond}}(r)$ results exhibit distinctive bimodal peaks. However, under the typical disordered plastic flow state in Figs. 5(d, e), the $P_{\text{bond}}(r)$ results exhibit only one prominent peak. Interestingly, at the right terminus of S_1 , the $P_{\text{bond}}(r)$ results in Fig. 5(c) seem to be a transition between one peak and bimodal peaks.

To further understand the observed bimodal peaks around the Shapiro steps in Fig. 5, we prepare histograms of the bond angle $P_{\text{angle}}(\phi)$ also from the Delaunay triangulation [84], as presented in Fig. 6. The insert of Fig. 6(a) shows a local snapshot of particle positions, where the angle between the bond and the y axis is de-

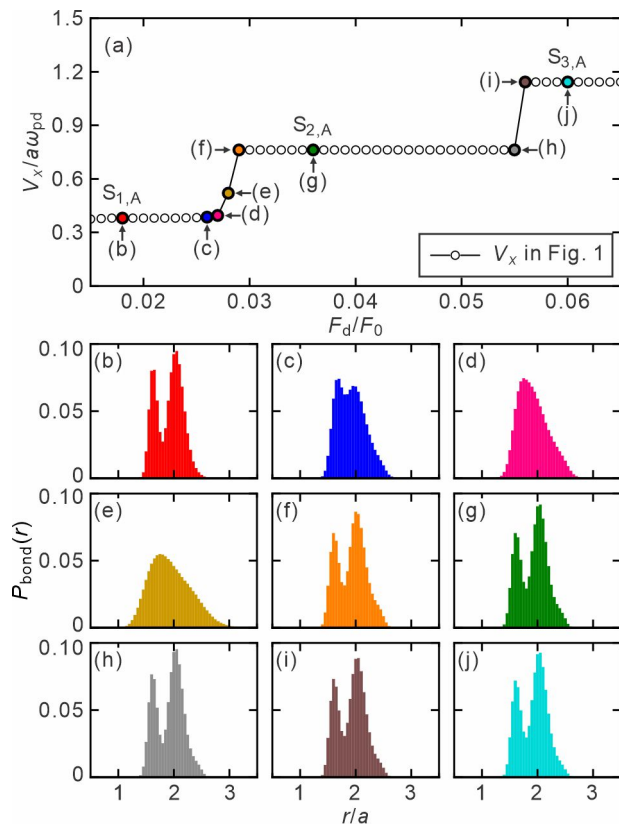


FIG. 5. Magnified view of the drift velocity V_x above (a), and histograms of the bond length $P_{\text{bond}}(r)$ (b-j). For the conditions of each Shapiro step, the $P_{\text{bond}}(r)$ results exhibit significant bimodal peaks as in panels (b, f, g, h, i, j). However, for the continuous transition conditions, the $P_{\text{bond}}(r)$ results exhibit only one prominent peak as in panels (d, e). For the conditions around the first Shapiro step terminus as in panel (c), the $P_{\text{bond}}(r)$ results exhibit mainly one peak with a slight feature of bimodal peaks, i.e., the combination of single and bimodal peaks.

finer as the bond angle ϕ . Clearly, as in Figs. 6(b, f, g, h, i, j), the $P_{\text{angle}}(\phi)$ results exhibit prominent bimodal peaks, located at $\phi \approx 0$ and $\approx \pi/3$, respectively, while the distribution between $\approx 0.1\pi$ and $\approx 0.25\pi$ is nearly zero. The prominent bimodal peaks in Figs. 6(b, f, g, h, i, j) clearly indicate the highly ordered structures under these conditions. For the typical disordered plastic flow state of Fig. 6(e), the bond angle is uniformly distributed, indicating the highly disordered state. Surprisingly, at the right terminus of S_1 , the $P_{\text{angle}}(\phi)$ result exhibits weaker bimodal peaks, with a wide distribution for all angles, as in Figs. 6(c, d), corresponding to the ordered structures with some disordered features.

Our observed bimodal-peak and one-peak features of $P_{\text{bond}}(r)$ in Fig. 5 can be well explained by the $P_{\text{angle}}(\phi)$ results in Fig. 6. Under the conditions of Shapiro steps in Figs. 6(b, f, g, h, i, j), the first peak of $P_{\text{angle}}(\phi)$ at $\phi \approx 0$ means that those bonds are nearly in the y directions, corresponding to the arrangement of 1D chains of parti-

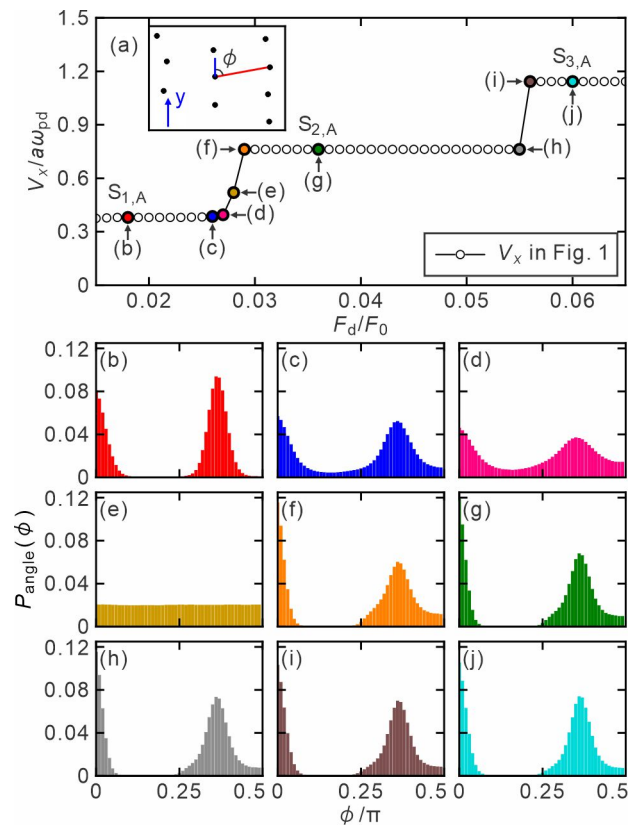


FIG. 6. Magnified view of the drift velocity V_x above (a), and histograms of the bond angle $P_{\text{angle}}(\phi)$ (b-j). The insert of panel (a) presents a typical snapshot of particle positions (dots) to indicate the definition of the angle ϕ of the bond between two neighbors relative to the y axis. For the conditions of each Shapiro step as in panels (b, f, g, h, i, j), the $P_{\text{angle}}(\phi)$ results exhibit significant bimodal peaks. For the continuous transition conditions as in panels (c, d), the $P_{\text{angle}}(\phi)$ results also exhibit weaker bimodal peaks with the widely distribution of all angles. For the conditions between Shapiro steps as shown in panel (e), $P_{\text{angle}}(\phi)$ results exhibit a nearly uniform value for all angles.

cles. The second peak at $\phi \approx \pi/3$ means the other bonds are mainly in the direction of $\pm\pi/3$, just corresponding to the stable zigzag structure, formed by neighboring particles from two adjacent 1D chains. We confirm that, under the conditions of the Shapiro steps in Fig. 5, for the bonds corresponding to the first peak of $P_{\text{bond}}(r)$, their angles are mostly $\phi \approx 0$. Similarly, the second peak of the $P_{\text{bond}}(r)$ also corresponding to the bonds whose angles are mostly $\phi \approx \pi/3$. As for the typical disordered plastic flow state of Fig. 6(e), the $P_{\text{angle}}(\phi)$ results remain constant, i.e., the bond angles are uniformly distributed, just due to the isotropic property of the highly disordered state. In Figs. 6(c, d), the $P_{\text{angle}}(\phi)$ results exhibit relatively low bimodal peaks, with the widely distribution of bond angles for all values, indicating the combination of the ordered and disordered states, probably leading to the continuous transition there.

To better characterize the 2D arrangement of particles

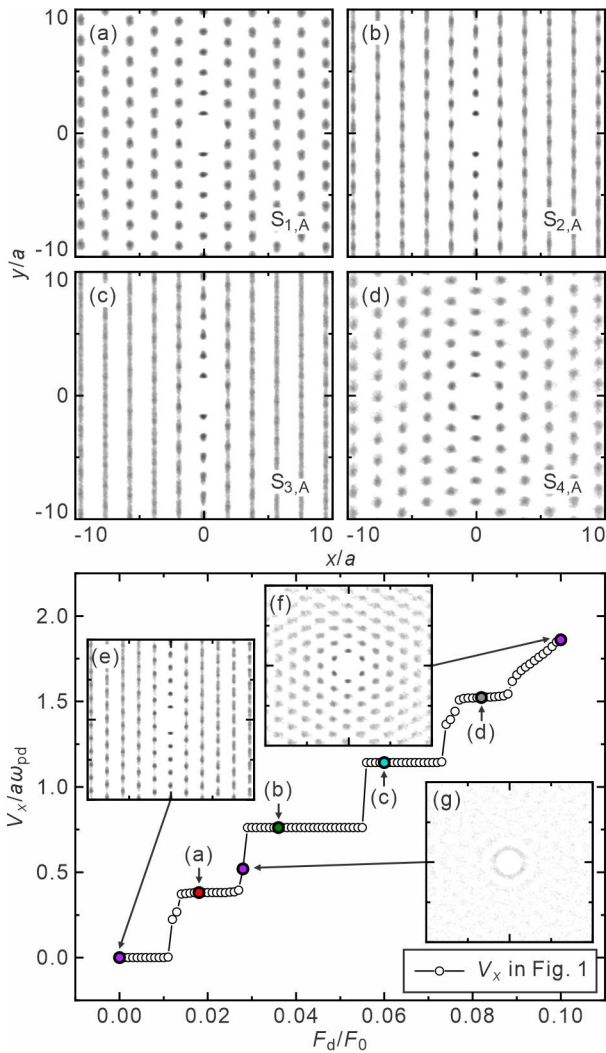


FIG. 7. Calculated 2D distribution functions G_{xy} of our studied 2D Yukawa solid under different conditions of $S_{1,A}$ (a), $S_{2,A}$ (b), $S_{3,A}$ (c), $S_{4,A}$ (d), $F_d/F_0 = 0.000$ (e), 0.028 (g), and 0.100 (f), respectively. Clearly, the hexagonal symmetry of the G_{xy} results in panels (a, d, f) means that particles are arranged in the highly ordered 2D triangular lattice. While the 1D structure of the G_{xy} results in panels (b, c, e) correspond to the ordered 1D chains. The circular distribution of the G_{xy} results in panel (g) clearly indicates the isotropic uniform distribution of the liquid state, corresponding to the disordered plastic flow state.

around these Shapiro steps, we calculate 2D distribution functions G_{xy} of our studied 2D system, as presented in Fig. 7. From Ref. [85], the G_{xy} function represents the probability of finding a particle at a specific location within a 2D plane relative to a central reference particle, which is powerful to characterize anisotropic systems. The G_{xy} results in Figs. 7(a, d, f) exhibit the hexagonal symmetry, indicating the highly ordered triangular lattice. The G_{xy} results in Figs. 7(b, c, e) exhibit the highly ordered structure along the y direction, indicating the 1D chains of the particle arrangement. For the typi-

cal disordered plastic flow state, the G_{xy} results exhibit the circular ring-shaped feature, clearly indicating the isotropic property of the highly disordered arrangement of particles, as in Fig. 7(g).

From our obtained G_{xy} results in Fig. 7, we speculate that the two types of the ordered structures of the particle arrangement maybe result in different behaviors observed on the Shapiro steps. Around both termini of S_1 and S_4 , the drift velocity V_x increases gradually, with the corresponding highly ordered triangular lattice with the hexagonal symmetry. However, at the transition between S_2 and S_3 , the drift velocity V_x changes abruptly from one step to the other without any intermediate data points at all. As compared with other transitions, the only characteristic is the structures of S_2 and S_3 are both ordered 1D chains. For our studied substrate-modulated Yukawa systems, it seems that any transitions around Shapiro steps either from or to the ordered triangular lattice is always continuous, however, the transition from one ordered 1D-chain structure to the other 1D-chain structure is discontinuous.

IV. SUMMARY

In summary, we perform Langevin dynamical simulations to study the depinning dynamics of a substrate-modulated 2D Yukawa solid driven by the uniform force. In our investigation, we specify a lateral periodic excitation $A \cos(2\pi f_s t)$ on the applied 1D substrate to introduce an additional frequency into the studied Yukawa system. Besides the previously found pinned, plastic flow, and moving ordered states, we also find that, when the ratio of the frequency from the drift motion over potential wells to the external frequency from modulation substrate is close to integers, dynamic mode locking occurs. As a result, we discover four prominent Shapiro steps from the overall drift velocity of particles.

We also perform systematic investigations of the structure and dynamics analysis of the 2D Yukawa system around Shapiro steps. From the dynamics analysis, we find that, under the conditions of Shapiro steps, the kinetic temperature $k_B T_y$ is significantly lower than the plastic flow state, clearly indicating the synchronization motion of all particles. From the global structural measure of sixfold coordinated particles P_6 , we find that, at the discovered Shapiro steps, our studied 2D Yukawa solid is highly ordered. Around both termini of the first and fourth Shapiro steps, the drift velocity increases gradually, corresponds to the continuous transitions. However, between the second and third Shapiro steps, the drift velocity changes from one to the other abruptly, without any data points between, which means the discontinuous transition there. We also prepare the histograms of the length and angle of the bond between neighboring particles under various conditions, which agree with the observed continuous/discontinuous transitions. From our calculated 2D distribution func-

tions, we speculate that the different ordered arrangements of particles probably result in the continuous or discontinuous transitions between the Shapiro steps and various depinning states.

Acknowledgments

The work was supported by the National Natural Science Foundation of China under Grant No. 12175159, the 1000 Youth Talents Plan, the Priority Academic Program Development of Jiangsu Higher Education Institutions, and the U. S. Department of Energy through the Los Alamos National Laboratory. Los Alamos National Laboratory is operated by Triad National Security, LLC, for the National Nuclear Security Administration of the U. S. Department of Energy (Contract No. 892333218NCA000001).

-
- [1] C. Reichhardt and C. J. O. Reichhardt, Pinning and dynamics of colloids on one-dimensional periodic potentials, *Phys. Rev. E* **72**, 032401 (2005).
- [2] K. Harada, O. Kamimura, H. Kasai, T. Matsuda, A. Tonomura, and V. V. Moshchalkov, Direct observation of vortex dynamics in superconducting films with regular arrays of defects, *Science* **274**, 1167 (1996).
- [3] A. Sengupta, S. Sengupta, and G. I. Menon, Driven disordered polymorphic solids: Phases and phase transitions, dynamical coexistence and peak effect anomalies, *Phys. Rev. B* **81**, 144521 (2010).
- [4] M.-C. Cha and H. A. Fertig, Peak Effect and the Transition from Elastic to Plastic Depinning, *Phys. Rev. Lett.* **80**, 3851 (1998).
- [5] W. Li, K. Wang, C. Reichhardt, C. J. O. Reichhardt, M. S. Murillo, and Y. Feng, Depinning dynamics of two-dimensional dusty plasmas on a one-dimensional periodic substrate, *Phys. Rev. E* **100**, 033207 (2019).
- [6] C. Reichhardt and C. J. O. Reichhardt, Depinning and nonequilibrium dynamic phases of particle assemblies driven over random and ordered substrates: A review, *Rep. Prog. Phys.* **80**, 026501 (2017).
- [7] T. Bohlein, J. Mikhael, and C. Bechinger, Observation of kinks and antikinks in colloidal monolayers driven across ordered surfaces, *Nat. Mater.* **11**, 126–130 (2012).
- [8] D. Mandelli, A. Vanossi, M. Invernizzi, S. Paronuzzi, N. Manini, and E. Tosatti, Superlubric-pinned transition in sliding incommensurate colloidal monolayers, *Phys. Rev. B* **92**, 134306 (2015).
- [9] C. Reichhardt and C. J. O. Reichhardt, Directional locking effects and dynamics for particles driven through a colloidal lattice, *Phys. Rev. E* **69**, 041405 (2004).
- [10] M. P. N. Juniper, A. V. Straube, R. Besseling, D. G. A. L. Aarts, and R. P. A. Dullens, Microscopic dynamics of synchronization in driven colloids, *Nat. Commun.* **6**, 7187 (2015).
- [11] Y. Wei and Y. Lei, Shapiro steps and chaos in the Frenkel-Kontorova model with substrate lateral vibration, *Phys. Rev. E* **106**, 044204 (2022).
- [12] J. Tekić and B. Hu, Properties of the Shapiro steps in the ac driven Frenkel-Kontorova model with deformable substrate potential, *Phys. Rev. E* **81**, 036604 (2010).
- [13] M. H. Jensen, P. Bak, and T. Bohr, Complete Devil’s Staircase, Fractal Dimension, and Universality of Mode-Locking Structure in the Circle Map, *Phys. Rev. Lett.* **50**, 1637 (1983).
- [14] Yu. M. Shukrinov, S. Yu. Medvedeva, A. E. Botha, M. R. Kolahchi, and A. Irie, Devil’s staircases and continued fractions in Josephson junctions, *Phys. Rev. B* **88**, 214515 (2013).
- [15] V. P. Singh, J. Polo, L. Mathey, and L. Amico, Shapiro Steps in Driven Atomic Josephson Junctions, *Phys. Rev. Lett.* **133**, 093401 (2024).
- [16] P. Martinoli, O. Daldini, C. Leemann, and B. Van den Brandt, Josephson Oscillation of a Moving Vortex Lattice, *Phys. Rev. Lett.* **36**, 382 (1976).
- [17] L. Van Look, E. Rosseel, M. J. Van Bael, K. Temst, V. V. Moshchalkov, and Y. Bruynseraede, Shapiro steps in a superconducting film with an antidot lattice, *Phys. Rev. B* **60**, R6998(R) (1999).
- [18] C. Reichhardt, R. T. Scalettar, G. T. Zimányi, and N. Grønbech-Jensen, Phase-locking of vortex lattices interacting with periodic pinning, *Phys. Rev. B* **61**, R11914(R) (2000).
- [19] G. Grüner, The dynamics of charge-density waves, *Rev. Mod. Phys.* **60**, 1129 (1988).
- [20] R. E. Thorne, J. S. Hubacek, W. G. Lyons, J. W. Lyding, and J. R. Tucker, Ac-dc interference, complete mode locking, and origin of coherent oscillations in sliding charge-density-wave systems, *Phys. Rev. B* **37**, 10055 (1988).
- [21] C. Reichhardt and C. J. Olson Reichhardt, Shapiro steps for skyrmion motion on a washboard potential with longitudinal and transverse ac drives, *Phys. Rev. B* **92**, 224432 (2015).
- [22] B. Hu and J. Tekić, Amplitude and frequency dependence of the Shapiro steps in the dc- and ac-driven overdamped Frenkel-Kontorova model, *Phys. Rev. E* **75**, 056608 (2007).
- [23] J. Beckers, J. Berndt, D. Block, M. Bonitz, P. J. Bruggeman, L. Couëdel, G. L. Delzanno, Y. Feng, R. Gopalakrishnan, F. Greiner, P. Hartmann, M. Horányi, H. Kersten, C. A. Knapek, U. Konopka, U. Kortshagen, E. G. Kostadinova, E. Kovačević, S. I. Krasheninnikov, I. Mann, D. Mariotti, L. S. Matthews, A. Melzer, M. Mikikian, V. Nosenko, M. Y. Pustyl’nik, S. Ratynskaia, R. M. Sankaran, V. Schneider, E. J. Thimsen, E. Thomas, H. M. Thomas, P. Tolia, and M. van de Kerkhof, Physics and applications of dusty plasmas: The Perspectives, *Phys. Plasmas* **30**, 120601 (2023).
- [24] H. M. Thomas and G. E. Morfill, Melting dynamics of a plasma crystal, *Nature (Lond.)* **379**, 806 (1996).

- [25] M. Bonitz, D. Block, O. Arp, V. Golubnychiy, H. Baumgartner, P. Ludwig, A. Piel, and A. Filinov, Structural Properties of Screened Coulomb Balls, *Phys. Rev. Lett.* **96**, 075001 (2006).
- [26] H. Kählert, J. Carstensen, M. Bonitz, H. Löwen, F. Greiner, and A. Piel, Magnetizing a Complex Plasma without a Magnetic Field, *Phys. Rev. Lett.* **109**, 155003 (2012).
- [27] V. Nosenko and J. Goree, Shear flows and shear viscosity in a two-dimensional Yukawa system (dusty plasma), *Phys. Rev. Lett.* **93**, 155004 (2004).
- [28] C. R. Du, V. Nosenko, H. M. Thomas, Y. F. Lin, G. E. Morfill, and A. V. Ivlev, Slow Dynamics in a Quasi-Two-Dimensional Binary Complex Plasma, *Phys. Rev. Lett.* **123**, 185002 (2019).
- [29] L. I. W. T. Juan, C. H. Chiang, and J. H. Chu, Microscopic particle motions in strongly coupled dusty plasmas, *Science* **272**, 1626 (1996).
- [30] A. Melzer, A. Homann, and A. Piel, Experimental investigation of the melting transition of the plasma crystal, *Phys. Rev. E* **53**, 2757 (1996).
- [31] J. H. Chu and L. I, Direct Observation of Coulomb Crystals and Liquids in Strongly Coupled rf Dusty Plasmas, *Phys. Rev. Lett.* **72**, 4009 (1994).
- [32] H. Thomas, G. E. Morfill, V. Demmel, J. Goree, B. Feuerbacher, and D. Möhlmann, Plasma Crystal: Coulomb Crystallization in a Dusty Plasma, *Phys. Rev. Lett.* **73**, 652 (1994).
- [33] R. L. Merlino and J. A. Goree, Dusty plasmas in the laboratory, industry, and space, *Phys. Today* **57**(7), 32 (2004).
- [34] V. E. Fortov, A. V. Ivlev, S. A. Khrapak, A. G. Khrapak, and G. E. Morfill, Complex (dusty) plasmas: Current status, open issues, perspectives, *Phys. Rep.* **421**, 1 (2005).
- [35] G. E. Morfill and A. V. Ivlev, Complex plasmas: An interdisciplinary research field, *Rev. Mod. Phys.* **81**, 1353 (2009).
- [36] A. Piel, *Plasma Physics* (Springer, Heidelberg, 2010).
- [37] M. Bonitz, C. Henning, and D. Block, Complex plasmas: A laboratory for strong correlations, *Rep. Prog. Phys.* **73**, 066501 (2010).
- [38] C. Liang, D. Huang, S. Lu, and Y. Feng, Determining global property of dusty plasma from single particle dynamics using machine learning, *Phys. Rev. Res.* **5**, 033086 (2023).
- [39] Y. Feng, J. Goree, and B. Liu, Solid Superheating Observed in Two-Dimensional Strongly Coupled Dusty Plasma, *Phys. Rev. Lett.* **100**, 205007 (2008).
- [40] E. Thomas, J. D. Williams, and J. Silver, Application of stereoscopic particle image velocimetry to studies of transport in a dusty (complex) plasma, *Phys. Plasmas* **11**, L37 (2004).
- [41] W. Yu, J. Cho, and J. C. Burton, Extracting forces from noisy dynamics in dusty plasmas, *Phys. Rev. E* **106**, 035303 (2022).
- [42] F. Wieben and D. Block, Entropy measurement in strongly coupled complex plasmas, *Phys. Rev. Lett.* **123**, 225001 (2019).
- [43] Y. He, B. Ai, C. Dai, C. Song, R. Wang, W. Sun, F. Liu, and Y. Feng, Experimental demonstration of a dusty plasma ratchet rectification and its reversal, *Phys. Rev. Lett.* **124**, 075001 (2020).
- [44] U. Konopka, G. E. Morfill, and L. Ratke, Measurement of the interaction potential of microspheres in the sheath of a rf discharge, *Phys. Rev. Lett.* **84**, 891 (2000).
- [45] Y. Feng, J. Goree, B. Liu, and E. G. D. Cohen, Green-Kubo relation for viscosity tested using experimental data for a two-dimensional dusty plasma, *Phys. Rev. E* **84**, 046412 (2011).
- [46] K. Qiao, J. Kong, J. Carmona-Reyes, L. S. Matthews, and T. W. Hyde, Mode coupling and resonance instabilities in quasi-two-dimensional dust clusters in complex plasmas, *Phys. Rev. E* **90**, 033109 (2014).
- [47] P. Hartmann, A. Z. Kovacs, A. M. Douglass, J. C. Reyes, L. S. Matthews, and T. W. Hyde, Slow Plastic Creep of 2D Dusty Plasma Solids, *Phys. Rev. Lett.* **113**, 025002 (2014).
- [48] A. Melzer, A. Schella, J. Schablinski, D. Block, and A. Piel, Instantaneous Normal Mode Analysis of Melting of Finite Dust Clusters, *Phys. Rev. Lett.* **108**, 225001 (2012).
- [49] Y. Feng, J. Goree, and B. Liu, Viscoelasticity of 2D Liquids Quantified in a Dusty Plasma Experiment, *Phys. Rev. Lett.* **105**, 025002 (2010).
- [50] Y. Feng, J. Goree, and B. Liu, Evolution of Shear-Induced Melting in a Dusty Plasma, *Phys. Rev. Lett.* **104**, 165003 (2010).
- [51] K. Jiang, Y. F. Li, T. Shimizu, U. Konopka, H. M. Thomas, and G. E. Morfill, Controlled particle transport in a plasma chamber with striped electrode, *Phys. Plasmas* **16**, 123702 (2009).
- [52] B. Liu, K. Avinash, and J. Goree, Transverse Optical Mode in a One-Dimensional Yukawa Chain, *Phys. Rev. Lett.* **91**, 255003 (2003).
- [53] Y. Feng, J. Goree, Z. Haralson, C.-S. Wong, A. Kananovich, and W. Li, Particle position and velocity measurement in dusty plasmas using particle tracking velocimetry, *J. Plasma Phys.* **82**, 615820303 (2016).
- [54] Y. Feng, J. Goree, and B. Liu, Accurate particle position measurement from images, *Rev. Sci. Instrum.* **13**, 10 (2007).
- [55] Y. Feng, J. Goree, and B. Liu, Errors in particle tracking velocimetry with high-speed cameras, *Rev. Sci. Instrum.* **82**, 053707 (2011).
- [56] Y. Zeng, Z. Ma, and Y. Feng, Determination of best particle tracking velocimetry method for two-dimensional dusty plasmas, *Rev. Sci. Instrum.* **93**, 033507 (2022).
- [57] A. Kananovich and J. Goree, Experimental determination of shock speed versus exciter speed in a two-dimensional dusty plasma, *Phys. Rev. E* **101**, 043211 (2020).
- [58] B. Liu and J. Goree, Superdiffusion and Non-Gaussian Statistics in a Driven-Dissipative 2D Dusty Plasma, *Phys. Rev. Lett.* **100**, 055003 (2008).
- [59] N. Yu, D. Huang, and Y. Feng, Melting curve of two-dimensional Yukawa systems predicted by isomorph theory, *Phys. Rev. E* **109**, 065212 (2024).
- [60] Y. Feng, B. Liu, and J. Goree, Rapid heating and cooling in two-dimensional Yukawa systems, *Phys. Rev. E* **78**, 026415 (2008).
- [61] D. Huang, M. Baggioli, S. Lu, Z. Ma, and Y. Feng, Revealing the supercritical dynamics of dusty plasmas and their liquidlike to gaslike dynamical crossover, *Phys. Rev. Res.* **5**, 013149 (2023).
- [62] S. Lu, D. Huang, C. Liang, and Y. Feng, Anelastic internal friction of dislocations in two-dimensional Yukawa

- solids, *Phys. Rev. Res.* **5**, 043116 (2023).
- [63] W. Zhu, C. Reichhardt, C. J. O. Reichhardt, and Y. Feng, Directional locking in a two-dimensional Yukawa solid modulated by a two-dimensional periodic substrate, *Phys. Rev. E* **106**, 015202 (2022).
- [64] L. Gu, W. Li, C. Reichhardt, C. J. O. Reichhardt, M. S. Murillo, and Y. Feng, Continuous and discontinuous transitions in the depinning of two dimensional dusty plasmas on a one-dimensional periodic substrate, *Phys. Rev. E* **102**, 063203 (2020).
- [65] Y. Huang, C. Reichhardt, C. J. O. Reichhardt, and Y. Feng, Superlubric-pinned transition of a two-dimensional solid dusty plasma under a periodic triangular substrate, *Phys. Rev. E* **106**, 035204 (2022).
- [66] Y. Huang, W. Li, C. Reichhardt, C. J. O. Reichhardt, and Y. Feng, Phonon spectra of a two-dimensional solid dusty plasma modified by two-dimensional periodic substrates, *Phys. Rev. E* **105**, 015202 (2022).
- [67] W. Li, D. Huang, C. Reichhardt, C. J. O. Reichhardt, and Y. Feng, The bifurcation structure of periodically forced current disruptions, *Phys. Rev. Res.* **5**, 023008 (2023).
- [68] G. J. Kalman, P. Hartmann, Z. Donkó, and M. Rosenberg, Two-Dimensional Yukawa Liquids: Correlation and Dynamics, *Phys. Rev. Lett.* **92**, 065001 (2004).
- [69] H. Ohta and S. Hamaguchi, Molecular dynamics evaluation of self-diffusion in Yukawa systems, *Phys. Plasmas* **7**, 4506 (2000).
- [70] K. Y. Sanbonmatsu and M. S. Murillo, Shear Viscosity of Strongly Coupled Yukawa Systems on Finite Length Scales, *Phys. Rev. Lett.* **86**, 1215 (2001).
- [71] B. Liu, J. Goree, V. Nosenko, and L. Boufendi, Radiation pressure and gas drag forces on a melamine-formaldehyde microsphere in a dusty plasma, *Phys. Plasmas* **10**, 9 (2003).
- [72] W. F. van Gunsteren and H. J. C. Berendsen, Algorithms for Brownian dynamics, *Mol. Phys.* **45**, 637 (1982).
- [73] P. Hartmann, G. J. Kalman, Z. Donkó, and K. Kutasi, Equilibrium properties and phase diagram of two-dimensional Yukawa systems, *Phys. Rev. E* **72**, 026409 (2005).
- [74] J. L. Abbott, A. V. Straube, D. G. A. L. Aarts, and R. P. A. Dullens, Transport of a colloidal particle driven across a temporally oscillating optical potential energy landscape, *New J. Phys.* **21**, 083027 (2019).
- [75] T. Brazda, C. July, and C. Bechinger, Experimental observation of Shapiro-steps in colloidal monolayers driven across time-dependent substrate potentials, *Soft Matter* **13**, 4024-4028 (2017).
- [76] C.-L. Wang, J. Tekić, W.-S. Duan, Z.-G. Shao, and L. Yang Existence and stability of the resonant phenomena in the dc-and ac-driven overdamped Frenkel-Kontorova model with the incommensurate structure *Phys. Rev. E* **84**, 046603 (2011).
- [77] J. Tekić, A. E. Botha, P. Mali, and Yu. M. Shukrinov, Inertial effects in the dc+ac driven underdamped Frenkel-Kontorova model: Subharmonic steps, chaos, and hysteresis, *Phys. Rev. E* **99**, 022206 (2019).
- [78] J. C. B. Souza, N. P. Vizarim, C. J. O. Reichhardt, C. Reichhardt, and P. A. Venegas, Shapiro steps and stability of skyrmions interacting with alternating anisotropy under the influence of ac and dc drives, *Phys. Rev. B* **110**, 014406 (2024).
- [79] N. P. Vizarim, C. Reichhardt, P. A. Venegas, and C. J. O. Reichhardt, Shapiro steps and nonlinear skyrmion Hall angles for dc and ac driven skyrmions on a two-dimensional periodic substrate, *Phys. Rev. B* **102**, 104413 (2020).
- [80] C. Reichhardt, R. T. Scalettar, G. T. Zimanyi, and N. Grønbech-Jensen, Shapiro steps in driven vortex lattices interacting with periodic pinning arrays, *Physica C* **332**, 1-4 (2000).
- [81] T. Klinger and A. Piel, The bifurcation structure of periodically forced current disruptions, *Phys. Scr.* **56**, 70-85 (1997).
- [82] J. Odavić, P. Mali, and J. Tekić, Farey sequence in the appearance of subharmonic Shapiro steps, *Phys. Rev. E* **91**, 052904 (2015).
- [83] M. P. N. Juniper, U. Zimmermann, A. V. Straube, R. Besseling, D. G. A. L. Aarts, H. Löwen, and R. P. A. Dullens, Dynamic mode locking in a driven colloidal system: experiments and theory, *New J. Phys.* **19**, 013010 (2017).
- [84] R. A. Quinn, C. S. Cui, J. Goree, J. B. Pieper, H. Thomas, and G. Morfill, Structural Analysis of a Coulomb Lattice in a Dusty Plasma, *Phys. Rev. E* **53**, R2049(R) (1996).
- [85] K. Loudiyi and B. J. Ackerson, Direct observation of laser induced freezing, *Physica A* **184**, 1 (1992).